Journal of Nanobiotechnology

RESEARCH

Open Access

Exploring the anti-inflammatory effects of curcumin encapsulated within ferritin nanocages: a comprehensive in vivo and in vitro study in Alzheimer's disease

Carlo Morasso[1], Marta Truffi[1], Veronica Tinelli[2], Polychronis Stivaktakis[3], Rosalinda Di Gerlando[4,5], Dragoni Francesca[5], Giulia Perini[5], Mahvish Faisal[6], Jana Aid[6], Bekzod Noridov[6], Benjamin Lee[6], Linda Barbieri[2], Sara Negri[1], Dragana Nikitovic[7], Lydia-Nefeli Thrapsanioti[7], Aristides Tsatsakis[3], Cristina Cereda[8,9], Arianna Bonizzi[1,8], Serena Mazzucchelli[8], Davide Prosperi[2], Miriam A. Hickey[6*], Fabio Corsi[1,8*] and Stella Gagliardi[5]

Abstract

Background The global demographic shift towards an aging population is generating a rise in neurodegenerative conditions, with Alzheimer's disease (AD) as the most prominent problem. In this landscape, the use of natural supplements has garnered attention for their potential in dementia prevention. Curcumin (Cur), derived from *Curcuma longa*, has demonstrated promising pharmacological effects against AD by reducing the levels of inflammatory mediators. However, its clinical efficacy is hindered by poor solubility and bioavailability. Our study introduces the use of H-Ferritin nanocages (HFn) as a nanoformulation vehicle for Cur, aiming to enhance its therapeutic potential for AD. In this work, we characterized a nanoformulation of Cur in HFn (HFn-CUR) by evaluating its safety, stability, and its transport across the blood-brain barrier (BBB) in vitro. Moreover, we evaluated the efficacy of HFn-CUR by transcriptomic analysis of peripheral blood mononuclear cells (PBMCs) from both AD patients and healthy controls (HC), and by using the well-established 5xFAD mouse model of AD.

Results Our data show that HFn-CUR exhibits improved water dispersibility, is non-toxic, and can traverse the BBB. Regarding its activity on PBMCs from AD patients, HFn-CUR enhances cellular responses to inflammation and reduces RAGE-mediated stress. Studies on an AD mouse model demonstrate that HFn-CUR exhibits mild beneficial effects on cognitive performance. Moreover, it effectively reduces microgliosis and astrogliosis and in vivo in mouse, suggesting potential neuroprotective benefits.

Conclusions Our data suggest that HFn-CUR is safe and effective in reducing inflammation in both in vitro and in vivo models of AD, supporting the need for further experiments to define its optimal use.

*Correspondence:
Miriam A. Hickey
miriam.ann.hickey@ut.ee
Fabio Corsi
fabio.corsi@icsmaugeri.it

Full list of author information is available at the end of the article

Graphical abstract

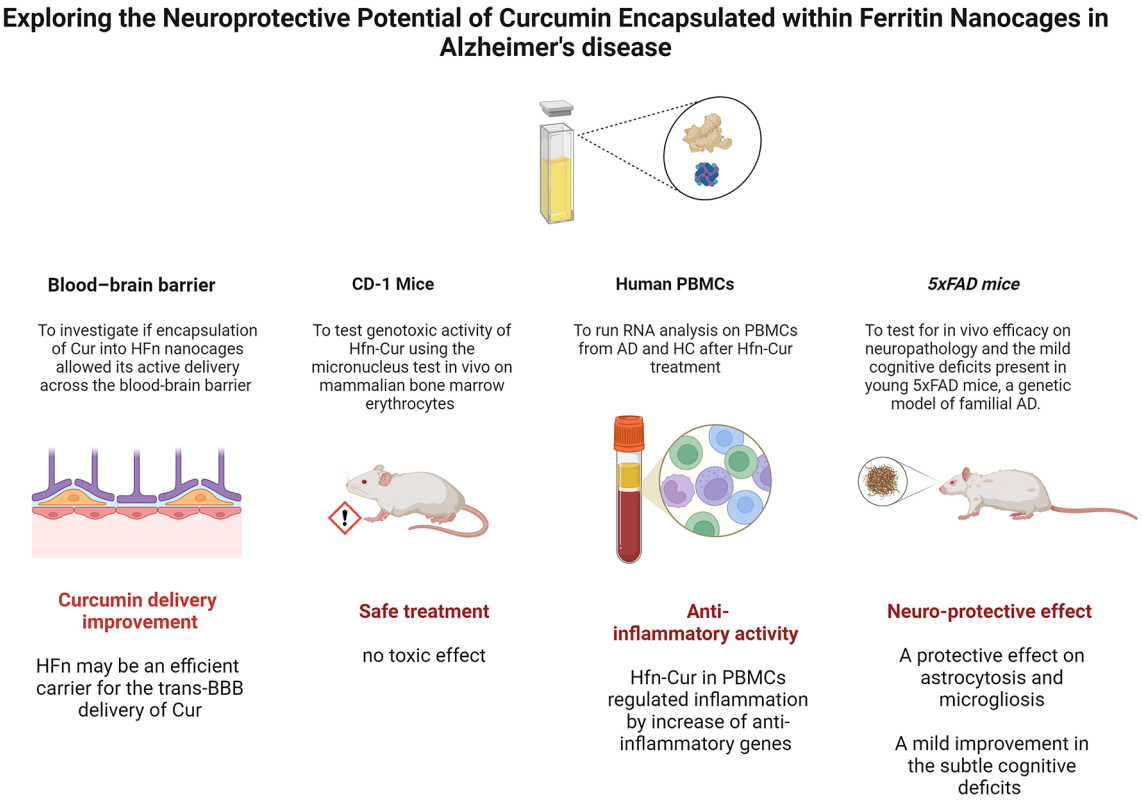

Keywords Curcumin, Nanoparticles, Alzheimer's disease, H-Ferritin, Blood-brain barrier, 5xFAD mice, Toxicity, Neuroinflammation

Background

The world's population is currently undergoing a rapid shift towards an increasingly aged population, a phenomenon that is contributing to a widespread decline in cognitive abilities. Alzheimer's disease (AD) stands as one of the preeminent causes of this deterioration. Despite the advent of new immune-based therapies, current treatment are not curative and their relevance to the millions of AD patients worldwide remain unclear [1].

The principal characteristic of AD is the cerebral accumulation of beta-amyloid (Aβ) plaques and tau fibrils. However, research consistently reveals that 20 to 30% of healthy elderly individuals also exhibit a significant presence of amyloid (Aβ) deposits with a reported relationship between Aβ deposition and measures of cognitive decline [2, 3]. With the anticipated increase in AD prevalence, the burden on national healthcare systems is expected to intensify. Consequently, the development of new therapies, particularly those targeting the initial stages of the disease process or aiming to prevent the disease, is urgent.

To address this clinical necessity, the utilization of natural supplements may represent a promising strategy for the prevention of dementia. This approach is associated with a growing awareness of the significance of nutrition in maintaining health [4, 5]. Among the various natural products investigated, several research groups have observed that *Curcuma longa* exhibits beneficial pharmacological effects on AD, both in vitro and animal models [6, 7]. In particular, curcumin (Cur) was shown to reduce the natural tendency of Aβ to aggregate in vitro, facilitating its removal by the immune system [8]. Evidence also indicates that Cur is effective in diminishing the levels of inflammatory mediators, and its anti-inflammatory properties may exert a positive impact on various diseases, including AD [9]. Indeed, central inflammatory microglia and astrocytes are widely recognized for their association with AD plaques [10], though their contributions to plaque clearance and maturation may differ [11]. Astrocyte polygenic risk scores correlate with amyloid fibril load [11], and research into AD risk genes has identified multiple genes expressed in microglia. For instance, a loss-of-function mutation in the Trem2 gene within

microglia is known to elevate the risk of AD and seems to amplify the amyloid-mediated aggregation of tau [12]. The anti-inflammatory effects of Cur in the periphery have been well-documented in the literature, particularly regarding the regulation of cytokines and transcription factors, such as NF-κB [13]. Furthermore, studies in cellular and animal models reported that Cur not only attenuates the formation of Aβ plaques but also promotes their decomposition and reduces the phosphorylation of tau [8, 14].

Clinical trials on humans, however, did not provide such clear evidence of Cur's protective effects. The challenge lies in the fact that Cur is entirely insoluble in water at pH levels below 7 and rapidly deteriorates in alkaline conditions. Furthermore, the bioavailability of Cur is notably low [15]. Therefore, it is improbable that Cur alone can offer substantial benefits. In all clinical trials where some benefits were observed, Cur was administered as a nanoformulation [5].

In this context, we present the application of H-Ferritin nanocages (HFn) as a nanoformulation of curcumin (HFn-CUR) for potential therapeutic use in AD.

Composed of 24 self-assembled H-ferritin monomers, HFn nanocages have a hollow structure with several clinically appealing features: (i) uniform architecture, (ii) minimal immunogenicity, and (iii) stability in physiological conditions [16]. Moreover, HFn naturally targets the transferrin receptor 1 (TfR1) [17], enabling it to traverse the Blood-Brain Barrier (BBB) and deliver drugs directly to the central nervous system (CNS) [18, 19]. Previous research has established a protocol for efficiently encapsulating Cur within HFn, significantly increasing its solubility and chemical stability [20]. Herein, we present a preliminary study that supports the application of HFn-CUR for the early treatment of AD.

To improve the translational potential of our novel formulation, we conducted an exhaustive characterization of the nanoformulation, assessing its toxicology and stability. Subsequently, we evaluated its transport across the BBB in vitro. Our efficacy assessment was twofold: first, through transcriptomic analysis of peripheral blood mononuclear cells (PBMCs) from AD patients and healthy controls (HC); second, by utilizing the well-established 5xFAD mouse model of AD [21], which harbors five mutations known to cause familial AD in humans. This model shows very early plaque accumulation and astrocyte and microglial activation [21] and does not show severe cognitive deficits until mid-life [22–24]. To further increase the translational relevance of our data, our in vivo work was based upon a thorough prior analysis of sample sizes and power analyses [24, 25]. Overall, our data suggest that HFn-CUR is safe and efficacious in reducing inflammation in vitro and in vivo models of AD.

Methods

Nanoformulation and characterization of HFn-CUR

The preparation of HFn-CUR nanoparticles followed a protocol previously described [20] based on the alkaline disassembly/reassembly strategy [26]. In brief, a solution of HFn (1 mg/mL, NaCl 150 mM) was adjusted to pH 12.5 by adding 1 M NaOH and stirring for 15 min. Purified Cur (see suppl. info.) was dissolved in 0.1 M NaOH at a concentration of 300 µM, and immediately introduced to the disassembled HFn. Afterwards the pH was promptly re-neutralized with 1 M HCl. The resulting solution was stirred for 2 h at room temperature to facilitate the reassembly of drug-loaded protein. Subsequently, the solution underwent centrifugation through a 100-KDa Amicon filter, followed by multiple washes with 20 mM phosphate buffer at pH 7.2. Final purification was achieved using Zeba Spin Desalting Columns to eliminate excess free Cur and adsorbed molecules. TEM electron microscopy was employed to confirm the correct formation of the HFn-CUR complexes.

The quantity of loaded Cur was determined spectroscopically by measuring the absorbance at 423 nm, following the method outlined by Pandolfi et al. [20]. To determine Cur loading, a calibration curve was initially constructed using various concentrations of the drug dissolved in acetic acid. An aliquot of the obtained HFn-CUR was diluted in acetic acid, and the pH was adjusted to 2, releasing the encapsulated Cur from the nanoparticles, the absorbance of which was subsequently measured spectroscopically.

In vitro blood-brain barrier study

To investigate the capability of HFn-CUR to cross the BBB, we conducted an in vitro transmigration assay, adapted from a previously published protocol [19]. Primary rat-brain microvascular endothelial cells (RBMEC) and rat cortical astrocytes (RCA), purchased from Innoprot (Derio, Spain), were co-cultured on polyethylene terephthalate transwell membranes (pore size 0.4 µm, 4.2 cm2 area, Corning) coated on the upper side with F/C, while the underside was coated with poly-L-lysine, as described above. RCA ($1\times10^{\wedge5}$ cells) were seeded onto the bottom side of the filter previously coated with poly-L-lysine (100 µg/mL, P1274, Sigma-Aldrich) for 1 h at room temperature and allowed to adhere for 4 h. Inserts were then placed into a 6-well plate containing 2 mL of Endothelial Cell Medium, supplemented with 5% fetal bovine serum, 1% endothelial cell growth supplement, 1% penicillin/streptomycin (sECM, Innoprot) and maintained at 37 °C and 5% CO_2 in a humidified atmosphere. The following day, RBMEC ($3\times10^{\wedge5}$ cells) were seeded onto the upper side of the filter coated with a solution of fibronectin (50 µg/mL, F1141, Sigma-Aldrich) and collagen IV (100 µg/mL, C5533, Sigma Aldrich) (F/C) in

1 mL of sECM supplemented with 1.4 µM hydrocortisone. Three inserts were left with RCA only to be used as control. From day 4 after co-culture, the transepithelial electrical resistance (TEER) was measured with an electrode device (EVOM2, World Precision Instruments). For each transwell, the mean TEER value of the inserts with RCA only was subtracted from the TEER value of the BBB, and the results were expressed as $\Omega \times cm^2$. The measurements were repeated every day until the TEER stopped increasing. To prove the integrity of the BBB model, the trans-permeability of the fluorescent tracer FITC-Dextran (FD40, molecular weight 40,000, Sigma-Aldrich) was measured on three BBB inserts. FD40 (1 mg/mL) was diluted in sECM and added in the upper chamber. At 1 and 2 hours, 200 µL were withdrawn from the lower chamber and analyzed by spectrofluorometry (λex=488 nm, λem=515 nm). A calibration curve was performed using 7-point concentrations of FD40 diluted in sECM.

To perform the trans-BBB study, 14 inserts were used for RBMEC and RCA co-culture. At day 12, when the BBB was established, HFn-CUR (100 µg/mL) or an equal concentration of free Cur was diluted in 1 mL of culture medium and incubated in the upper chamber. The medium in the lower chamber was replaced with 2 mL of fresh sECM. Two BBB inserts were incubated with sECM without HFn-CUR or Cur and used as blank controls. At 3 and 7 h, all media in the upper and lower chambers were collected and stored at − 80 °C for UPLC/MS-MS measurement. After wash with phosphate buffer saline with calcium and magnesium (PBS Ca/Mg), RBMEC were detached from the insert with 300 µL of trypsin/EDTA, collected in 1.5 mL tubes, and centrifuged for 5 min at 500 ×g. Cell pellets were washed twice with PBS Ca/Mg and stored at -80 °C for analysis by UPLC/MS-MS (see Suppl. Info: Determination of Curcumin).

Libraries preparation for RNA-Seq and bioinformatic data analysis

Sequencing libraries of the treated and untreated PBMCs from AD patients and matched controls (see Suppl. Info: PBMCs Isolation, Treatment, and RNA Extraction) were prepared with the Illumina TruSeq Stranded RNA Library Prep kit, version 2, Protocol D, using 500 ng total RNA. The quality of the sequencing libraries was assessed by the 2100 Bioanalyzer with a DNA1000 assay and DNA High-Sensitivity assay. RNA processing was carried out using Illumina NextSeq 500 Sequencing. FastQ files were generated via Illumina bcl2fastq2 starting from raw sequencing reads produced by an Illumina NextSeq sequencer. Gene and transcript intensities were computed using STAR/RSEM software (1.3.3), Madison, WI, USA [27] using Gencode Release 19 (GRCh37.p13) as a reference and using the "stranded" option. A differential expression analysis for mRNA was performed using R package EBSeq [28]. This tool was selected because of its superior performance in identifying isoform differential expressions [29]. Differential expression analysis for long noncoding RNAs was performed with the R package DESeq.2 [30]. Coding and noncoding genes were considered differentially expressed and retained for further analysis with $|\log2(\text{disease sample/healthy control})| \geq 1$ and an FDR≤0.1. A gene enrichment analysis was performed on coding genes. We performed a gene ontology (GO) analysis for the biological processes, cellular components, and molecular function and a KEGG pathway analysis [31] via the enrichR web tool [32]. Gene enrichment analysis was performed on coding genes with Kegg pathway analysis [31] and enrichR web tool [32].

In vivo drug treatment

The mice were recruited in a staggered manner, from successive litters. Allocation to treatment groups was pseudorandomized to ensure littermate controls. Drug administration was not blinded; however, all behavioral testing and neuropathological analyses were conducted blinded.

Experimental mice were housed together in mixed genotype and treatment groups of 3–10. Cage positions remained constant throughout treatment. Mice were weighed and then treated twice weekly from 2 months of age until 4 months of age with 1 mg/kg HFn-CUR via intraperitoneal injections at a dose volume of 0.1 mg/ml. As our goal was to examine whether our nanoformulated version was of benefit in early AD, and as previous papers have studied the effects of unformulated curcumin in mouse models of AD [5], a curcumin-only group was not included. Control-treated WT and TG mice were housed together with HFn-CUR -treated TG mice; thus, the experimental unit was a mouse. Stock solutions of HFn-CUR were stored in the dark at -80 °C and then diluted in sterile saline for administration. Control mice received saline only. The side of injection (right lower abdomen, left lower abdomen) was alternated for each successive injection and the order of injections varied. Mice exhibiting stereotypy (continuously doing backflips or jumping) were excluded from the preclinical trial. Additional mice that were excluded included one WT and one TG saline-treated mouse that lost weight during treatment and that were euthanised early, $N=4$ mice that did not demonstrate sufficient visual acuity during the visual learning protocol of Morris water maze testing and $N=1$ mouse where the genotype did not match the original. The final group sizes were $N=16$ saline-treated WT, $N=10$ saline-treated TG, $N=11$ HFn-CUR -treated TG, which provided excellent power to detect treatment effects on neuropathology [24], our primary outcome measure.

Morris water maze

Morris water maze testing was used to uncover treatment effects on subtle learning deficits in mice at 4 months of age. Cognitive performance was tested during the final 3 weeks of treatment, as previously described [24]. Briefly, mice were brought through visual-spatial learning (4 trials per day, over a period of 5 days, starting and platform positions varied with trial) [33]. Training for subsequent spatial learning took place over 4 trials per day for 6 days. On the 7th day, the platform was removed to test memory in a single trial (spatial probe trial). Training for reversal learning then took place over 4 trials per day for 6 days followed on the 7th day by a single reversal probe trial. During spatial learning, the platform was in the southwest quadrant. For reversal learning, the platform was in the northeast quadrant. Ethovision XT V8 (Noldus, Wageningen, Netherlands) was used to monitor learning and swimming patterns.

Inflammation examination

Inflammation was examined based upon anti-GFAP and anti-IBA1 immunohistochemistry on two cryosections (approx. 3.1 mm lateral of bregma) per mouse.

Anti-IBA1: sections were processed as previously described [24]. Sections from 2 × WT mice were lost during processing. Control sections were run in parallel that were not exposed to primary antibody, and no specific staining was observed in these sections.

Anti-GFAP: sections were processed as described previously [24]. Sections from 1 × WT mouse were lost during processing. Hoechst staining was used to confirm anatomical position of RoIs. For imaging, Z-stacks were taken of regions of interest (RoIs) at 20× using an LSM 780 confocal microscope (through the entire depth of the region of interest, using the 561 nm laser only (ex 561 nm, em 578–696 nm). The percent area covered by anti-GFAP signal was used as the outcome measure. For morphological analysis of astrocytes in subiculum, high-resolution Z-stacks were taken at 40×, and Maximum intensity projections were limited to 20× Z-steps due to the density of astrocytes in this RoI. These maximum intensity projections were then batch-processed in ImageJ (FIJI) using macros. Following the isolation of individual astrocytes from the processed images, Sholl analysis (from the image) was conducted using the ImageJ (FIJI) Neuroanatomy plugin, using 5 µm step sizes for the radii. The mean number of intersections per shell per mouse was used to generate group means for comparison (see Suppl. Info: Statistical analysis).

Results

Characterization of HFn-CUR

To address the issue of the limited water solubility of Cur, we employed a nanoformulation made of previously described H-ferritin nanocages [20]. Employing a gentle method of pH-guided disassembly/reassembly of ferritin monomers, we successfully loaded Cur into the nanoparticle core, resulting in a clear HFn-CUR aqueous suspension (Fig. 1A). TEM analysis affirmed the structural integrity of the HFn-CUR (Fig. 1B) particles, and DLS was used to confirm the absence of aggregates in the dispersion [20].

A spectroscopic method was utilized to assess the efficiency of Cur loading within HFn nanocages and the formulation's stability over time. Notably, examination of the percentage of encapsulated Cur retained within the nanocage core at physiological pH (pH=7.2) revealed the presence of a minor fraction of the drug (approximately 15–20%) that was adsorbed onto the surface of HFn nanocages. This fraction was rapidly released within approximately 2 h. In contrast, most Cur remained securely encapsulated within the nanocage core and was only released in slightly acidic conditions (Fig. 1C) [34].

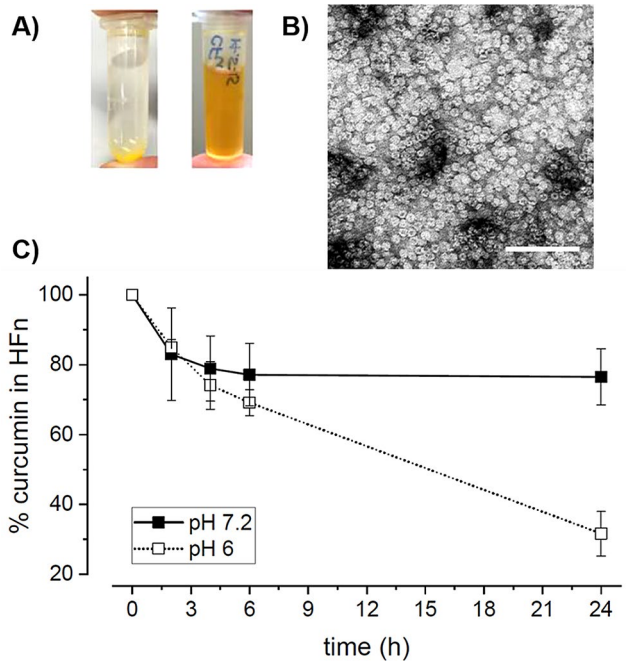

Fig. 1 **A**) Comparison of curcumin dispersion: On the left, water-dispersed Cur settles at the bottom of the flask, on the right, well-dispersed HFn-CUR. **B**) TEM images depict HFn-CUR, affirming the structural integrity of the HFn. **C**) Time-release profile of Cur from HFn-CUR: Black squares represent release at neutral pH, while white squares denote release in slightly acidic conditions

Micronucleus assay in mouse bone marrow

To evaluate the toxicological profile of HFn-CUR, three distinct batches were prepared and tested for their impact on erythropoiesis in the bone marrow of CD-1 mice, compared with free Cur. The results, summarized in Table 1, revealed that the ratio of polychromatic

Table 1 Effects of three different batches of HFn-CUR or free curcumin on erythropoiesis in the bone marrow of CD-1 mice

	PCEs/(PCEs + NCEs) % ± SD	*P* (t-test)
Control	0.55 ± 0.03	
HFn-CUR 01	0.52 ± 0.02	0.240
HFn-CUR 02	0.54 ± 0.04	0.773
HFn-CUR 03	0.51 ± 0.05	0.329
Cur	0.51 ± 0.06	0.372

Table 2 Micronuclei (MN) frequencies with the corresponding standard deviation (sd) and p values (t test) for all experimental groups compared with the control

	MN PCEs ± sd	*P* (t-test)
Control	7.33 ± 1.53	
HFn-CUR 01	11.33 ± 1.53	0.201
HFn-CUR 02	9.33 ± 1.53	0.494
HFn-CUR 03	12.33 ± 1.53	0.121
Cur	7.00 ± 0.00	0.901

erythrocytes (PCEs) to the sum of PCEs and normochromatic erythrocytes (NCEs) together was not statistically different between control and exposed groups.

Furthermore, as illustrated in Table 2, upon examination of micronucleus frequencies (MN) in each experimental group, no statistically significant differences were discerned in MN among the exposure groups ($p > 0.05$) when compared to the control group. These outcomes prove the lack of genotoxic effects associated with HFn-CUR exposure.

Micronucleus assay in human blood lymphocytes

The analysis of the micronucleus (MN) assay in peripheral blood lymphocyte cultures is detailed in Table 3, which provides essential metrics such as the average frequency of binucleated cells with micronuclei (BNMN), the mean frequency of micronuclei with standard deviation, and the p-value reflecting the comparison between the experimental and control groups. Additionally, the table presents the Cytokinesis Block Proliferation Index (CBPI) along with its associated standard deviation.

These data show that no statistically significant differences in frequency of micronuclei and binucleated cells with micronuclei (BNMN) were discerned across all tested concentrations when compared to the control group ($p > 0.05$). Furthermore, the evaluation of CBPI revealed no statistically significant difference between the control and exposed groups. This observation suggests that there are no observable cytotoxic effects induced by the tested batches of HFn-CUR.

Curcumin transport across an in vitro blood brain barrier (BBB) model

It was previously described that HFn nanocages can be used for the delivery of molecules and also antibodies to the central nervous system [35, 36]. To investigate whether HFn encapsulation allowed the active delivery of Cur across the BBB, we conducted a transmigration assay in vitro. The assay consisted of a two-compartment in vitro BBB system with a transwell insert. The insert was coated with primary RBMEC on the upper side and with RCA on the underside, to form a tight endothelial monolayer supported by astrocytes that model the physiological fidelity of the BBB. The integrity of the BBB model and its ability to block high molecular weight molecules were assessed by TEER and apparent permeability measurements (Figure S1). HFn-CUR or free Cur were added to the upper chamber diluted in the culture medium and, after 3–7 h of incubation, the medium was collected from the lower chamber to measure the amount of Cur that permeated across the BBB system. Following treatment with free Cur, only small traces were found in the lower chamber at both 3 and 7 h. By contrast, HFn-CUR significantly enhanced permeation across the BBB: Cur concentration measured in the lower chamber at 3 h was significantly increased in HFn-CUR as compared to free Cur, and this effect intensified after 7 h of incubation (Fig. 2A).

Moreover, we examined the uptake of Cur by the endothelial cells of the BBB system upon HFn-CUR or free Cur exposure. An extremely low fraction of free Cur was internalized by RBMEC after 3 and 7 h of incubation. In contrast, the nanoformulation triggered a significant cell uptake of Cur thanks to the recognition of HFn by the TfR1 receptor on the surface of endothelial cells (Fig. 2B). This observation indicated that HFn facilitated the entry

Table 3 Statistical assessment of the MN assay in peripheral blood lymphocyte cultures includes the mean frequency of BNMN, the mean frequency of MN, the CBPI, and the corresponding standard deviation

	BNMN ± sd	*P* (t-test)	MN ± sd	*P* (t-test)	CBPI
Control	7.0 ± 0.5		8.0 ± 1.0		1.86 ± 0.02
HFn-CUR 01 5 µg/ml	6.0 ± 0.5	0.697	9.0 ± 1.5	0.728	1.85 ± 0.03
HFn-CUR 01 10 µg/ml	7.0 ± 1.0	1.000	9.0 ± 0.5	0.728	1.84 ± 0.02
HFn-CUR 02 5 µg/ml	9.0 ± 1.5	0.468	11.0 ± 1.0	0.314	1.85 ± 0.02
HFn-CUR 02 10 µg/ml	10.0 ± 0.5	0.285	12.0 ± 1.5	0.186	1.84 ± 0.02
HFn-CUR 03 5 µg/ml	6.0 ± 1.0	0.697	8.0 ± 1.0	1.000	1.85 ± 0.04
HFn-CUR 03 10 µg/ml	8.0 ± 0.5	0.711	10.0 ± 1.5	0.494	1.86 ± 0.03

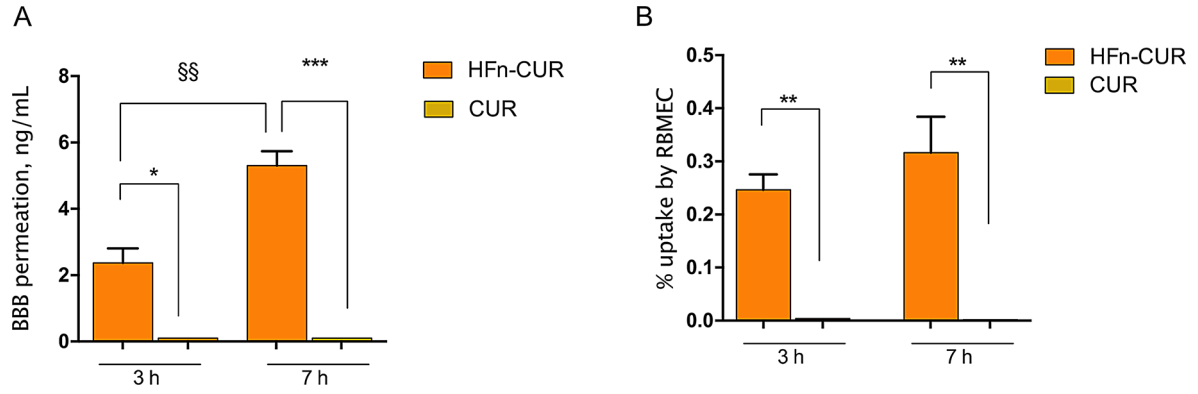

Fig. 2 **A**) Concentration of Cur measured in the lower compartment of BBB transwells after 3- and 7-hours incubation with HFn-CUR or free Cur equally dosed at 0.1 mg/mL. **B**) Percent uptake of HFn-CUR or free Cur by RBMEC cells. Reported values are the mean or at least 3 replicates. Statistical analysis was done by unpaired t-test: * $p < 0.05$; ** $p < 0.01$; ***$p < 0.0005$ HFn-CUR vs. free CUR; §§ $p < 0.01$ 3 vs. 7 h

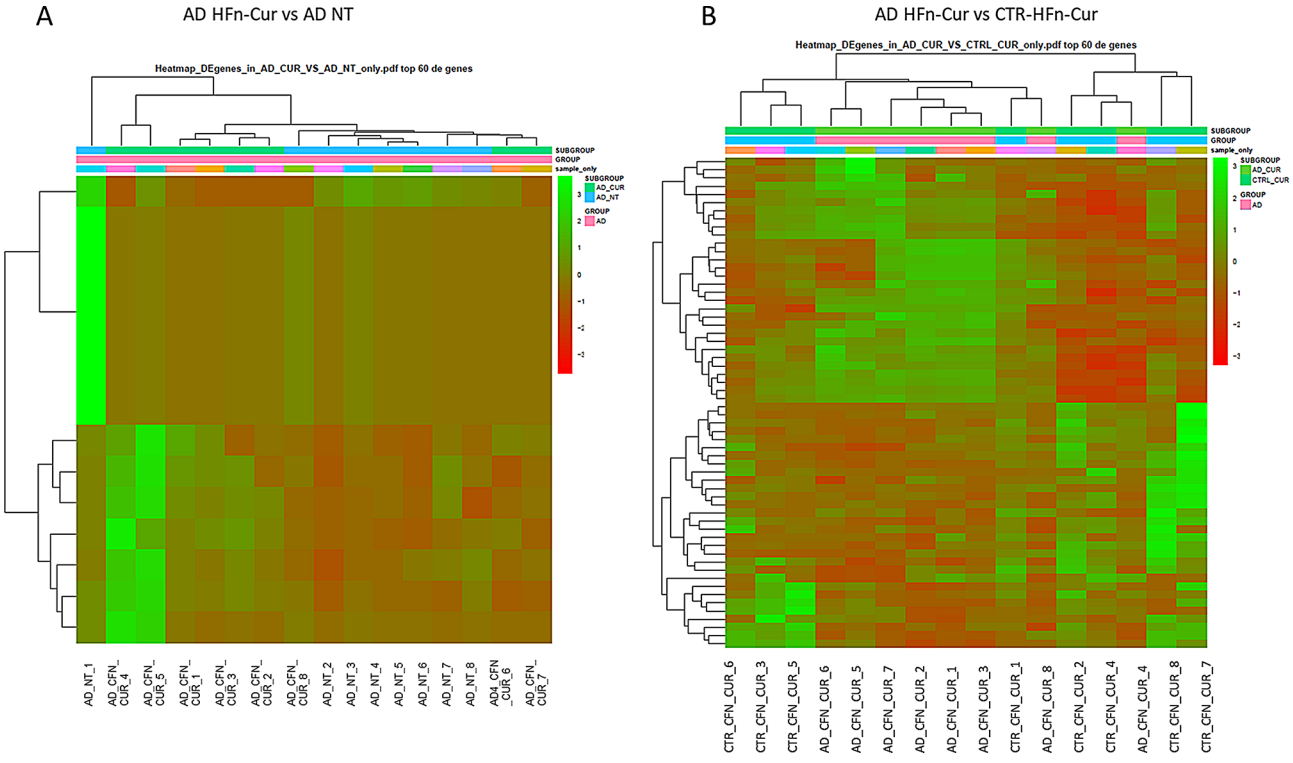

Fig. 3 Expression profiles of differently expressed genes in AD and healthy controls. In panel **A**), differentially expressed (DE) mRNAs between HFnCurAD vs. ntAD are shown, while in panel **B**) DE HFnCurAD vs. HFnCurHC are shown by Heatmap. All comparisons are given between the disease state and the control samples. We considered as differentially expressed only genes showing |log2(disease sample/healthy donor) | ≥1 and a False Discovery Rate ≤ 0.1

of Cur into the endothelial cells of the BBB, confirming an active trans-cellular delivery of HFn-CUR.

RNAseq analysis of differentially expressed mRNAs and lncRNAs in HFn-treated PBMCs

We investigated the effects of HFn-CUR treatment on the differential expression of RNAs by looking at four distinct conditions: untreated PBMCs, from Alzheimer's disease patients (ntAD), PBMCs from Alzheimer's patients treated in vitro with HFn-CUR (HFnCurAD), untreated PBMCs from healthy controls (ntHC), and PBMCs from healthy controls treated in vitro with HFn-CUR (HFnCurHC) (Fig. 3A, B).

Multiple differently expressed genes (DE) were found in the different comparisons, as summarized in Table 4. As previously reported [6], we identified 630 deregulated mRNAs when comparing ntAD and ntHC. When we compared HFnCurHC with ntHC, we observed variations in the expression levels of 771 genes, with 181 up-regulated and 590 down-regulated compared with ntHC.

Table 4 Statistically significant differentially expressed mRNAs and lncRNAs number in PBMCs from AD patients, in terms of up-regulated transcripts, down-regulated transcripts and total. Counts are reported for AD not treated (ntAD) versus controls not treated (ntHC), ntAD versus AD treated with Hfn-CUR (HFnCurAD), AD and HD treated with HFn-CUR (HFnCurAD vs. HFnCurHC) and ntHC versus HfnCurHC. Transcripts were considered as differentially expressed when |log2(disease sample/healthy control)|≥1 and a FDR ≤ 0.1

	Up-regulated		Down-regulated		total RNAs
	mRNA	lncRNA	mRNA	lncRNA	
ntAD vs. ntHC	333	11	234	52	630
ntAD vs. HFnCurAD	21	2	8	9	31
HFnCurAD vs. HFnCurHC	550	13	496	81	1140
ntHC vs. HFnCurHC	151	30	566	24	771

In stark contrast, when we compared HFnCurAD with ntAD, only 31 genes exhibited altered mRNA counts (23 up-regulated and 17 down-regulated) (Table 4, Table S4). This discrepancy underscores a marked difference in the treatment's effectiveness in PBMCs isolated from AD subjects compared to those from HC. To further emphasize this disparity, we compared the differential gene expression between HFnCurAD and HFnCurHC, revealing alterations in 1140 RNAs.

Pathway analysis of RNAseq data from HFn-treated PBMCs

We thus extended our inquiry into the underlying pathways associated with these gene expression changes. Pathway analysis revealed specific influences on immune-related processes in the comparison of ntAD with HFnCurAD. Specifically, we observed the activation of cytokines and chemokines, as well as RAGE receptor binding (Fig. 4A). Within these pathways, alterations were observed in CXCL1 and CXCL5, EGF factors, and chemokine receptors. Additionally, interleukin-mediated signalling pathways were found to be altered. Pertaining to biological processes, pathways related to cytokine secretion and the migration of granulocytes and leukocytes were also implicated (Fig. 4B).

The pathway analysis investigation of the differentially expressed (DE) genes obtained by comparing HFnCurAD and HFnCurHC revealed an involvement of lipid activity and integrin binding, while inflammatory pathways were not significantly deregulated (Fig. 4C). Regarding biological processes, the data of particular interest showed an involvement of leukocyte and lymphocyte activation. Additionally, pathways related to lipid metabolism (such as localization, transportation, and metabolic processes) were also identified (Fig. 4D). The comparison between ntHC and HFnCurHC revealed differences in terms of tyrosine kinase activity, splice site binding, and lipid binding. However, GO enrichment did not reveal

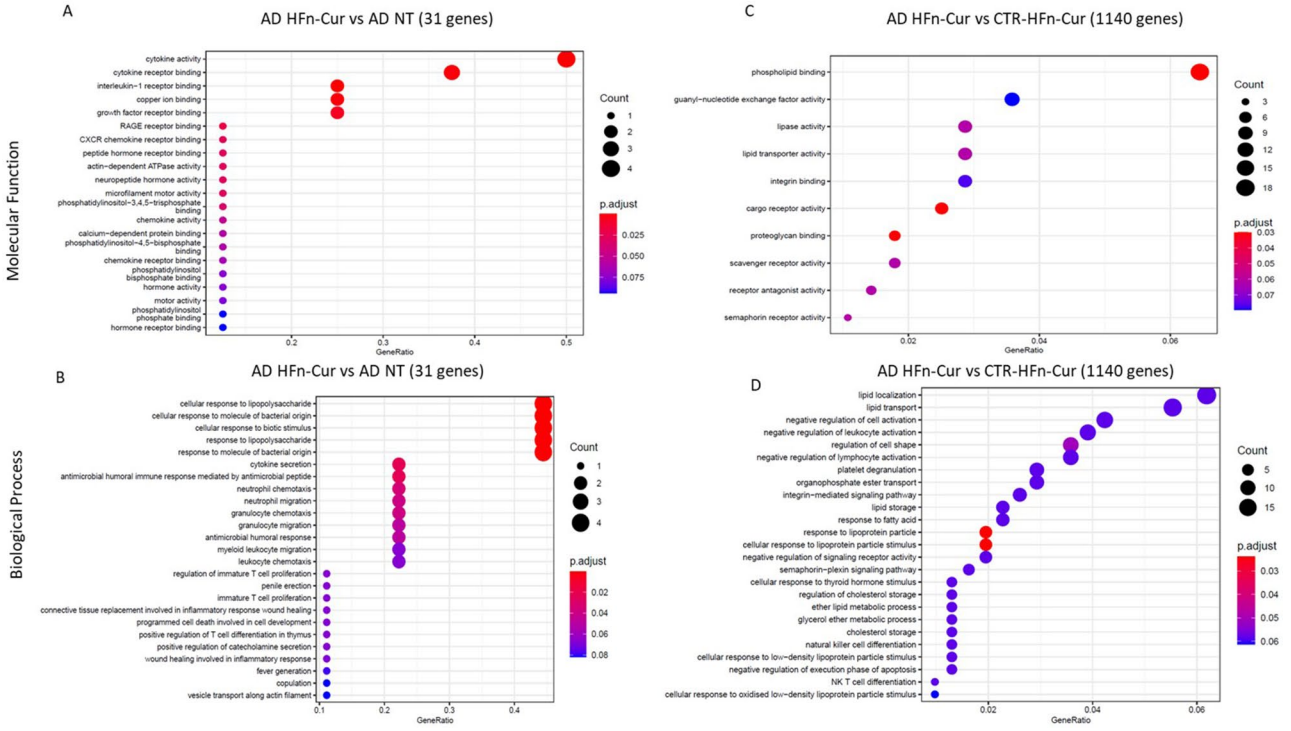

Fig. 4 GO Pathway analysis. Molecular Function and Biological process analysis of deregulated genes for HFnCurAD vs. ntAD (**A**, **B**) and HFnCurAD vs. HFnCurHC (**C**, **D**)

alterations in pathways that may be directly linked to AD pathology or immune response (Figure S2).

Effects of HFn on general health and behaviour in an in vivo model of AD

Mice were treated twice weekly with 1 mg/kg of HFn-CUR via intraperitoneal injections for 2 months, from 2 to 4 months of age. In line with toxicological data, body weight analysis indicated that the treatment was well-tolerated. Saline treated WT mice, saline-treated TG and HFn-CUR-treated TG mice exhibited similar body weights throughout the 2-month treatment period (Suppl Fig. 3A). This observation reaffirmed the absence of treatment-related toxicity, as indicated by the 2-way ANOVA showing a lack of effect of treatment in TG mice (Effect of treatment F (1, 19)=0.07, ns). Saline-treated TG mice were similar to saline-treated WT mice (effect of genotype, F (1, 24)=1.1, ns). Open-field activity assessments showed no significant differences in activity levels between saline-treated TG and WT mice saline (Suppl Fig. 3B, 2-way ANOVA effect of genotype F (1, 24)=0.3 ns; C, 2-way ANOVA effect of genotype F (1, 24)=0.06). These findings were in line with previous studies by our group and by others [22, 24], which demonstrated that the activity of 5xFAD TG mice remained normal between 2 and 4 months of age (Suppl. Fig S3 B, C). Open-field activity was normal also in HFn-CUR-treated TG mice (Suppl. Fig S3 B, 2-way ANOVA effect of treatment F (1, 19)=0.8 ns; C, 2-way ANOVA effect of treatment F (1, 19)=0.8, ns). This result reinforced the absence of any adverse effects attributed to HFn-CUR treatment (Suppl. Fig. S3 B, C). We have previously conducted thorough testing of cognition in 5xFAD TG mice. Cognitive deficits are quite mild at this age, and only become severe by approximately 1 year of age [24]. By treating mice of this age it was thus possible to obtain information on the possible protective effects of HFn-CUR at very early stages of disease. Importantly, there were no genotype or treatment effects detected during visual-spatial (Suppl. Fig S3 D), spatial (Suppl. Fig S3 E) or reversal (Suppl. Fig S3 F) learning assessment in the Morris water maze test. However, we observed mild deficits in our saline-treated TG mice because their quadrant occupancies (Fig. 5B) were less efficient than in saline-treated WT mice (Fig. 5A). A beneficial effect of HFn-CUR in TG mice was detected as the HFn-CUR-treated TG group learned to focus on the correct quadrant by day 5, while saline-treated TG mice reached this level of efficiency by day 6 (Fig. 5A-C). Memory for the platform positions was tested in probe trials demonstrating no overall differences between groups, yet saline-treated TG mice tended to focus less on the correct quadrant following spatial and reversal learning. However, following spatial learning (Fig. 5D) and reversal learning (Fig. 5E), HFn-CUR-treated TG mice showed superior performance in quadrant differentiation compared to saline-treated TG mice. WT mice showed excellent differentiation of the correct quadrant (Fig. 5D). Importantly, no differences in swim speed were observed between groups. Overall, our data show very mild cognitive deficits in 5xFAD TG mice at these young ages. Nevertheless, in these secondary outcome measures, preference for the correct quadrant tended to be strongest in saline-treated WT mice and HFn-CUR-treated TG mice, compared with saline-treated TG mice.

Neuropathological outcomes were the primary outcome of the study performed on mice

There is no evidence of neuronal loss in 5xFAD transgenic mice until approximately 9 months of age, and then, only in cortical layer [5]. Volume loss tends to occur in thalamus and hypothalamus, in particular in 14-month-old transgenic mice, with no change in hippocampus [37]. Some synaptic loss has been reported in medial prefrontal cortex of 6-month-old male transgenic 5xFAD mice with concomitant loss of mitochondria [38]. Similarly, a very mild reduction in functional mitochondria in hippocampus was noted in 6-month-old transgenic mice (sex unknown) [39]. An imaging surrogate for oxidative stress only became consistently different from normal mice by 8 months of age, with HNE immunocytochemistry not increased until approximately 12 months [40]. We therefore examined inflammation and plaques, to adhere to current known translationally relevant biomarkers.

Analysis of amyloid deposition, performed using antibody-based staining (MOAB2), Thioflavin S, and Congo Red, did not reveal any significant effects of HFn-CUR treatment (Suppl Fig S4 A, B, C). (MOAB2: effect of treatment F (1, 19)=0.7. ns; ThioS: effect of treatment F (1, 19)=0.4, ns; Congo red: F (1, 18)=0.07, ns).

Amyloid-induced microglia activation in AD leads to the development of disease-associated microglial (DAM) [41, 42]. Cur is well known as an anti-oxidant agent [5]. We thus tested the possible effect of HFn-CUR treatment on microgliosis and astrogliosis on the 5xFAD TG mice as they develop robust microgliosis and astrogliosis starting from approximately 2 months of age [21].

To evaluate the impact of HFn-CUR treatment on microglia, particle analysis was employed, considering the larger and more activated morphology of TG microglia (2-way ANOVA, WT saline vs. TG saline, F (1, 22)=49.4, $p<0.0001$). Comparing TG groups, HFn-CUR reduced microglial particle size in frontal somatosensory cortex, with an effect size of 1.2, but not in subiculum (Fig. 6A). Concerning inflammation, GFAP-positive astrocytes were absent in WT somatosensory cortex, but as expected, were abundant in the cortex of saline-treated TG mice [21]. In contrast, GFAP-positive astrocytes were detected in subiculum of WT mice at this age, but again,

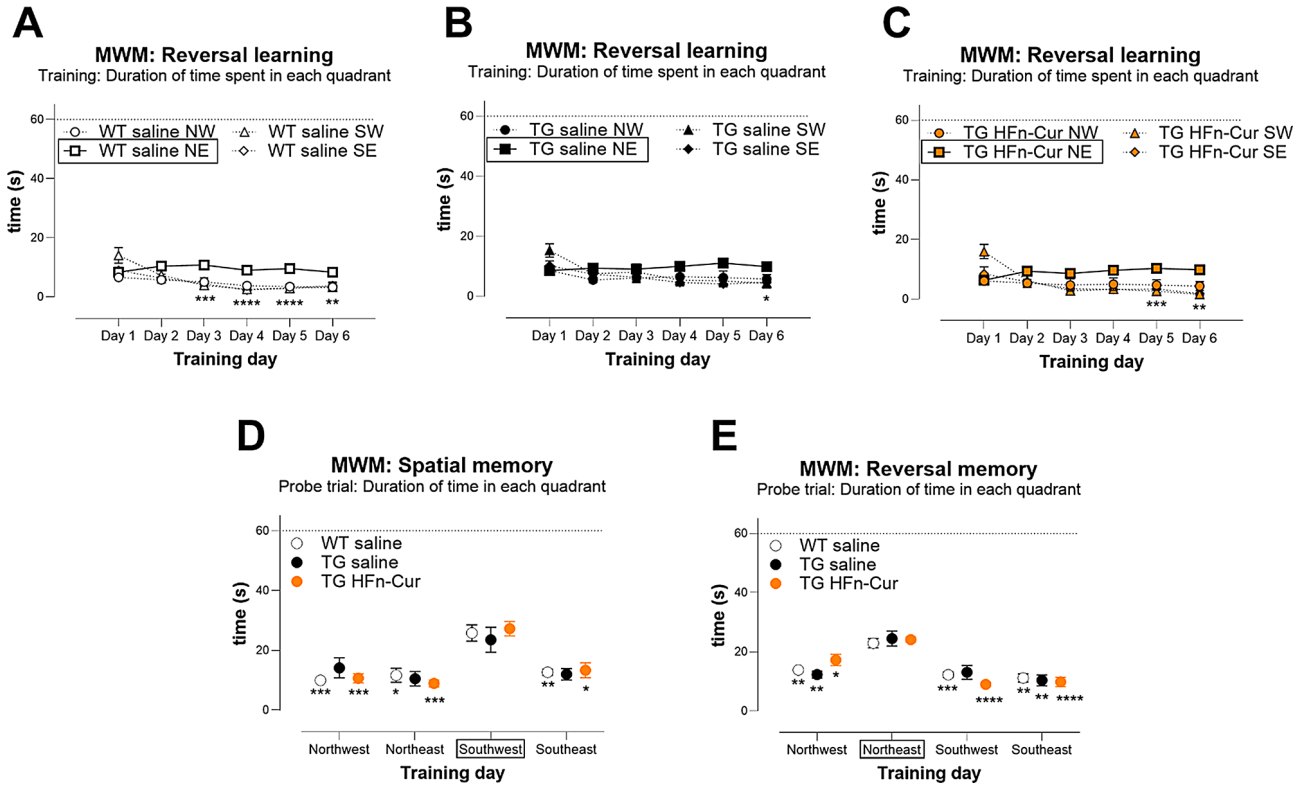

Fig. 5 Morris water maze. Although saline-treated WT mice showed excellent location to the correct quadrant (**A**), saline-treated TG mice only learned the correct quadrant by day 6 (**B**) whereas HFn-CUR-treated TG mice learned this by day 5 (**C**). When testing memory during probe trials, again, the ability to focus upon the correct quadrant was consistently best in saline-treated WT mice and HFn-CUR-treated TG mice, followed by saline-treated TG mice during probe testing of spatial memory (**D**) with a similar pattern observed during reversal memory testing (**E**). A: 2-way ANOVA, day x quadrant interaction: WT saline F (2.3, 34.0) = 7.6, $p < 0.002$; B: 2-way ANOVA, day x quadrant interaction: TG saline F (3.7, 33.6) = 5.4, $p < 0.003$; C: 2-way ANOVA, day × quadrant interaction: HFn-Cur TG F (2.2, 21.5) = 9.3, $p < 0.002$); D: 2-way ANOVA effect of quadrant WT saline versus TG saline F (1.7, 39.9) = 10.6; 2-way ANOVA effect of quadrant TG saline versus TG HFn-Cur F (2.1, 39.7) = 11.5, $p < 0.0001$; E: reversal probe test, 2-way ANOVA effect of quadrant WT saline versus TG saline F (2.3, 54.1) = 20.1 $p < 0.0001$; 2-way ANOVA effect of quadrant TG saline versus TG HFn-Cur F (2.2, 42.7) = 21.7 $p < 0.0001$). Symbols are of group mean ± sem. A, B, C: * $p < 0.05$, ** $p < 0.01$, *** $p < 0.001$ only when correct quadrant occupation (NE, denoted by box) was significantly different to all three other quadrants. G, H: * $p < 0.05$, ** $p < 0.01$, *** $p < 0.001$, *** $p < 0.0001$ compared with same-group, correct quadrant. Correct quadrant denoted by box (E: SW; E: NE)

we detected far more, activated, astrocytes in subiculum of saline-treated TG mice. The complete statistical analysis is reported in table S3.

HFn-CUR treatment did not specifically affect frontal cortex astrogliosis but significantly reduced it in the subiculum with an effect size of 1 (Fig. 6B; saline-treated TG 95% CI 7.5–11.5, HFn-CUR-treated TG 95% CI 4.6–8.5). Moreover, there was an overall effect of treatment, with HFn-CUR-treated TG mice showing reduced astrocytic load in general (TG saline versus TG HFn-CUR, 2-way ANOVA overall effect of treatment F (1, 19) = 5.8, $p < 0.03$). Astrocyte individual morphology was also analysed in subiculum. As expected, astrocytes in TG mice treated with saline were larger than those in WT mice, indicating activation (radius x genotype interaction, F (6, 132) = 21.6, $p < 0.0001$). HFn-CUR reduced astrocyte size in TG mice, suggesting partial normalisation Fig. 6C (radius x treatment interaction, F (6, 110) = 3.025 $p < 0.01$). Critically, these specific areas (frontal cortex for microglia, subiculum for astrocytes) had been selected previously as having the highest power to detect treatment effects [24].

Discussion

The potential therapeutic application of Cur as an anti-inflammatory agent, which may be advantageous in treating cognitive decline and neurodegeneration, has been extensively debated within the scientific community. While numerous studies suggest the efficacy of this compound in in vitro models [8, 43], the data from clinical trials in humans, particularly in patients with Alzheimer's disease, have not yielded positive results [44, 45]. This lack of clear beneficial outcomes in clinical settings has led some researchers to doubt the overall pharmacological effectiveness of Cur and the debate on the possibility to use Cur as therapeutic agent is still ongoing [46, 47]. To address this issue, the development of Cur nanoformulations has been proposed to enhance the

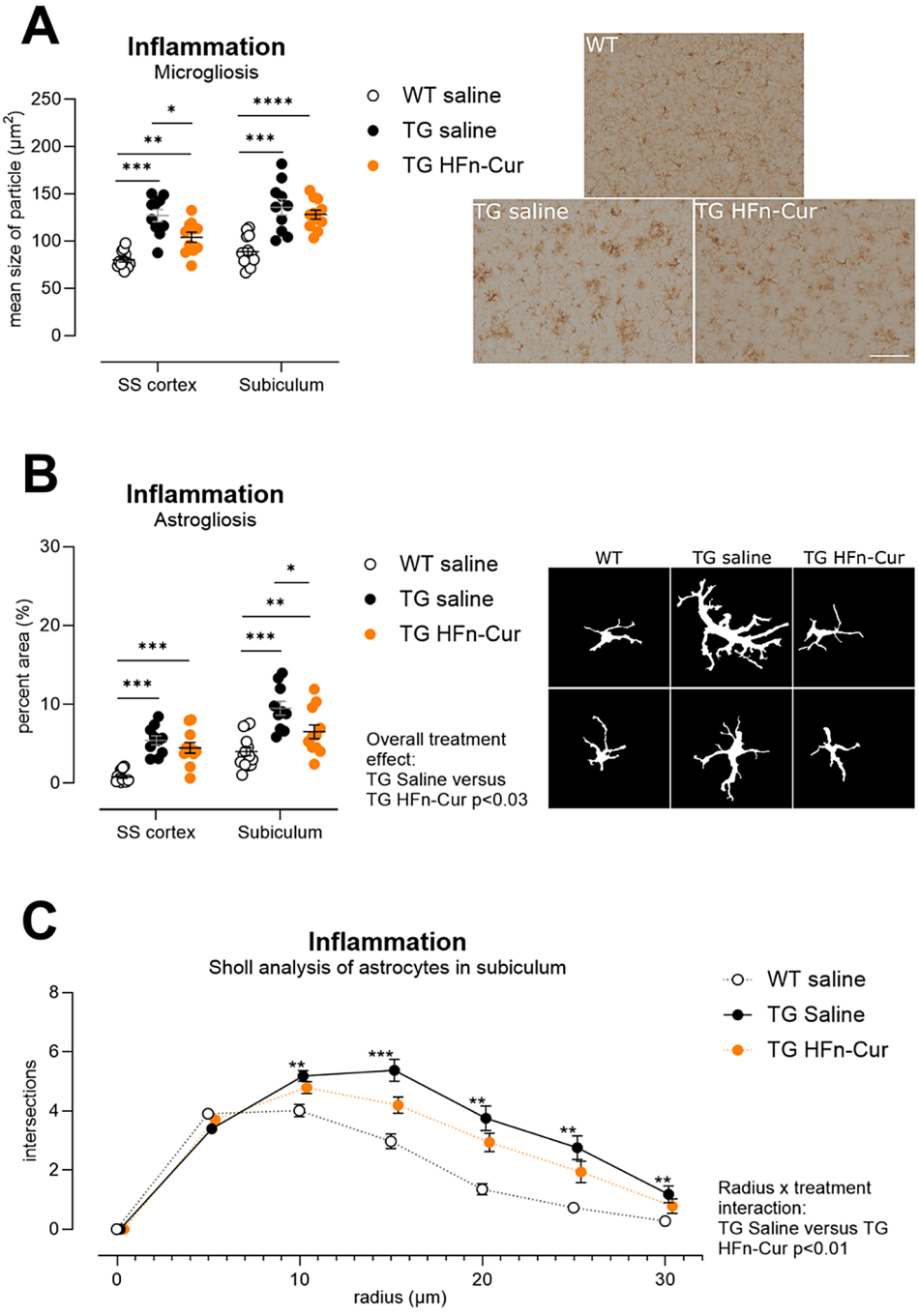

Fig. 6 Inflammation. Microgliosis (**A**): Treatment with HFn-CUR reduced microglial size in frontal somatosensory cortex but not in subiculum. Photomicrographs depict somatosensory cortex of a saline-treated WT (top), saline-treated TG (lower left) and HFn-CUR-treated TG (lower right) mouse. Scale-bar = 100 µm. Frontal cortex: TG saline 95% CI: 112–142, TG HFn-Cur 95% CI: 93–116. * $p < 0.05$, ** $p < 0.01$, *** $p < 0.001$. Astrocytosis (**B**): HFn-CUR treatment resulted in an overall reduction in GFAP-positive astrocytes compared with saline-treated TG mice, with post-hoc testing revealing a specific effect in subiculum (**B**). Saline-treated TG 95% CI 7.5–11.5, HFn-CUR-treated TG 95% CI 4.6–8.5. ** $p < 0.01$, *** $p < 0.0001$. Morphological analysis of astrocytes in subiculum revealed a partial normalisation of astrocyte morphology in HFn-CUR-treated TG mice (**C**). Black and white images show representative astrocytes used for morphological analysis (saline-treated WT: left column, saline-treated TG: middle column; HFn-CUR-treated TG: right column). Each image is 80 µm x 80 µm. Symbols in graphs are of individual mice together with group mean ± sem (**A**,**B**) or of group mean ± sem (C, where there are no error bars, they are obscured behind symbols). ** $p < 0.01$, *** $p < 0.001$ compared with WT saline

compound's stability and water solubility. Notably, Pandolfi et al. previously developed a Cur nanoformulation utilizing ferritin nanoparticles, which they evaluated in the context of triple-negative breast cancer [20]. In our study, we explore the potential effects of Cur encapsulated within ferritin nanoparticles (HFn-CUR) in both in vitro and in vivo models related to Alzheimer's dementia and cognitive impairment. Given ferritin's ability to cross the blood-brain barrier (BBB), we anticipated that this nanoformulation could be particularly beneficial for the treatment of neurological diseases. The prepared Hfn-CUR was examined to check its characteristics, to ensure its lack of toxicity and to investigate its pharmacological properties and its role in regulating gene and protein expression both in vivo and in vitro.

HFn-CUR exhibited remarkable water dispersibility, in stark contrast to the inherent hydrophobicity of free Cur. This dispersibility is attributed to the molecule's encapsulation within the central cavity of the nanoformulation, with only approximately 10% of the drug being adsorbed on the outer surface and promptly released. HFn-Cur selectively releases its Cur payload within a mildly acidic environment, aligning with the pH of astrocytes [34] and the lysosomal compartment of e.g., immune cells [48].

The obtained results proved that HFn-CUR does not exhibit cytotoxic effects on erythropoiesis in the bone marrow of CD-1 mice. The ratio of polychromatic erythrocytes (PCEs) to the sum of PCEs and normochromatic erythrocytes (NCEs), as well as the frequencies of micronuclei and binucleated cells with micronuclei (BNMN), showed no statistically significant differences between the control and exposed groups. This aligns with the findings of previous studies on Cur-loaded nanoparticles [49, 50]. For instance, a study on Cur-loaded amphiphilic poly-N-vinylpyrrolidone nanoparticles demonstrated that these nanoparticles were safe for healthy cells and showed high cytotoxicity for glioblastoma cells [49]. The micronucleus (MN) assay is a well-established method for evaluating genotoxic effects and it has been used widely for the evaluation of different compounds [51, 52].

Once we had confirmed the lack of toxicity of HFn-CUR, we investigated its ability to traverse the blood-brain barrier (BBB). The BBB, composed of tightly packed endothelial and supportive cells, regulates the passage of molecules into the brain, protecting it from potentially harmful substances. However, this barrier also poses a challenge for drug delivery to the brain, limiting the effectiveness of many therapeutic agents [53]. Overcoming this barrier is therefore essential for developing successful treatments for neurological disorders such as AD [54].

By using primary brain-derived cells, we established a BBB in vitro and tested the ability of HFn-CUR to traverse it in comparison to free Cur. HFn-CUR promoted the trans-BBB delivery of Cur, a significant advantage compared with free Cur, as demonstrated by the amount of drug that overcame the BBB in vitro. Importantly, HFn nanoparticles retain their natural ability to bind transferrin receptors, which are abundantly expressed on the surface of brain endothelial cells, and thus facilitate their active transport across the BBB [36, 54]. Indeed, in our study we found HFn-Cur in the endothelial BBB cells whereas cellular uptake of free Cur was not observed at the same dose and incubation time. This result indicated a specific mechanism of cell uptake and transcytosis that was driven by HFn nanoformulation. Leveraging their ability to navigate biological barriers, HFn nanoparticles promote Cur penetration into the BBB endothelium and guided its transcellular passage into brain. This "Trojan horse" approach enables efficient and targeted delivery of Cur across the BBB, enhancing its potential therapeutic efficacy in AD.

Peripheral cell have become important for the investigation of pathological mechanisms of neurodegenerative diseases and peripheral blood has been indicated as a potential source of biomarkers in AD [55, 56]. As we have already described [6], PBMCs are a very consistent and representative model for gene expression regulation in AD pathology. Here, we present a whole transcriptome profile in PBMCs from AD patients and matched controls that were treated in vitro with HFn-CUR to investigate gene regulation and identify altered pathways after treatment. In all groups analysed, we detected an important deregulation in mRNA expression, in particular when AD and matched controls, both treated, were compared.

HFn-CUR treatment increases the difference between AD and HC. HFn-CUR treatment seems to improve cell response to inflammation. In fact, Cur has long been recognized for its anti-inflammatory properties. The compound has shown promise in inhibiting key inflammatory pathways and reducing the production of pro-inflammatory molecules. Moreover, HFn-CUR demonstrates neuroprotective effects by decreasing Receptor for Advanced Glycation Endproducts (RAGE), a protein that usually increases in AD, and that interacts with Aβ leading to cell stress with the generation of reactive oxygen species [57]. Moreover, cytokines pathways are also involved in AD and our data showed a reduction in pro-inflammatory species. Biological processes showed involvement of inflammation with negative regulation of leukocyte and lymphocyte activation and this aspect aligns with the broad range of Cur action reported in the literature. Finally, our data showed that HFn-CUR showed a different effect on AD and HC cells after the same treatment, in fact, in samples from AD, the effect of HFn-CUR treatment compared to AD untreated was an alteration of only 31 genes, while in treated HC samples, we observed an important number of gene (771) changes.

This inconsistency highlights a notable variation in the efficacy of the treatment on PBMCs extracted from individuals with AD as opposed to those from HC. Several papers have been published on the relationship between Aβ and lipids, demonstrating that lipids, particularly cholesterol, may influence the processing and accumulation of Aβ [58, 59]. Our RNA-seq results show an alteration in both mechanisms related to lipid metabolism and inflammation, suggesting that treatment with HfN-CUR may help in restoring the pathological condition to a physiological one.

In vivo, HFn-CUR was non-toxic, as HFn-CUR-treated 5xFAD and TG mice gained weight in line with saline-treated TG and WT littermates, which is in keeping with our toxicological data in human blood lymphocytes and our micronucleus assay. Moreover, spontaneous activity was normal in 5xFAD TG mice at this age, and no deleterious effect on activity was noted in TG mice treated with HFn-CUR. As we have shown previously, using several different cognitive tests, cognition is only very mildly impaired at this age in 5xFAD TG mice, indeed, only Morris water maze has the sensitivity to detect genotype effects at these ages [24]. The Morris water maze is a very well-known test of cognitive function and several outcome measures are possible [33]. We provide Gallagher's proximity data here for completion, but as we have previously shown, the dynamic range of these data are very large [24], precluding our ability to detect genotype or treatment effects and limiting the use of this outcome measure. Quadrant occupancy is far less variable, and we noted that of our three treatment groups, saline-treated TG mice showed the worst search strategy when searching for the platform in the Morris water maze, with HFn-CUR TG mice performing at an intermediate level and saline-treated WT mice showing the best search strategy. Thus, we found a mild beneficial effect of HFn-CUR on cognitive performance, our secondary outcome. Our primary outcome was neuropathology. There is no evidence of neuronal loss in 5xFAD transgenic mice until approximately 9 months of age, and then, only in cortical layer [60]. Volume loss tends to occur in thalamus and hypothalamus, in particular in 14-month-old transgenic mice, with no change in hippocampus [37]. Thus, our data from 4-month-old transgenic mice are likely equivalent to FDA's draft guidance preclinical AD stage 2, where biomarkers are abnormal but individuals display subtle clinical signs (https://www.fda.gov/downloads/Drugs/GuidanceComplianceRegulatoryInformation/Guidances/UCM5967). This draft guidance was created to facilitate therapeutic studies aimed at earlier stages of disease. We believe our trial was ideally placed to interrogate this stage of disease. We did not note any effect of HFn-CUR on amyloid plaques; however, based upon studies of other nanoformulated formulations of Cur, it is possible that longer treatment times or higher concentrations are required [5] to disaggregate or prevent formation of beta-pleated sheets, as we were well-powered to detect 30% reduction in, e.g., subiculum. However, our formulation did reduce microgliosis in frontal cortex in 5xFAD TG mice and it also reduced astrogliosis in general, and had a specific effect in subiculum. Interestingly, we had identified microgliosis in frontal cortex and astrocytosis in subiculum, a priori, as having the highest power to detect treatment effects [24], with much greater sensitivity to treatment effects than plaques. Beta amyloid clearly activates microglia in AD but over time, and continued release of pro-inflammatory factors and reactive species by microglia likely contributes to oxidative stress [61]. Astrocytes upregulate their expression of GFAP and become activated in AD thereby contributing to the pro-oxidant environment [62]. Thus, although we treated for 2 months only, at a time likely to be equivalent to preclinical AD, our treatment effects are likely to be beneficial. Indeed, a small-molecule inhibitor of microglia reduced microglia, improved motor neuron count and improved motor coordination in a mouse model of tauopathy (P301S) [63] and as shown above, HFn-CUR, in particular, affected genes associated with inflammation. Critically, at higher concentrations, Cur by itself or in lipidated form reduces astrocytes and microglia in mouse models of AD [64, 65].

Conclusions

In summary, we have developed a nanoformulation of Cur encapsulated within ferritin nanoparticles (HFn-CUR) that holds promise for addressing the limitations of free Cur in treating Alzheimer's disease (AD). HFn-CUR exhibits improved water dispersibility, is non-toxic, and has the ability to traverse the blood-brain barrier. It enhances cellular responses to inflammation, reduces RAGE-mediated stress, and shows mild beneficial effects on cognitive performance. Although it does not directly impact amyloid plaques, it effectively reduces microgliosis and astrogliosis, suggesting potential neuroprotective benefits. Further investigations are warranted to optimize treatment duration and concentration for optimal outcomes in AD therapy.

Abbreviations

AD	Alzheimer's disease
Aβ	Beta-amyloid
Cur	Curcumin
HFn	H-Ferritin
HFn-CUR	Curcumin loaded H-Ferritin nanoparticles
BBB	Blood-brain-barrier
CNS	Central nervous system
PBMCs	Peripheral blood mononuclear cells
HC	Healthy controls
RBMEC	Rat-brain microvascular endothelial cells
RCA	Rat cortical astrocytes
sECM	Endothelial Cell Medium with supplements

TEER	Transepithelial electrical resistance
PBS	Phosphate buffer saline
GO	Gene ontology analysis
WT	Wild type
TG	Transgenic
PCEs	Polychromatic erythrocytes
NCEs	Normochromatic erythrocytes
MNPCEs	Micronuclei polychromatic erythrocytes
MN	Micronucleus
BNMN	Binucleated cells with micronuclei
CBPI	Cytokinesis Block Proliferation Index
ntHC	Untreated PBMCs from healthy controls
ntAD	Untreated PBMCs from Alzheimer's disease patients
HFnCurHC	PBMCs from healthy controls treated with HFn-CUR
HFnCurAD	PBMCs from Alzheimer's patients treated with HFn-CUR
mRNAs	Messenger RNA
lncRNAs	Long non-coding RNAs
DE	Differentially expressed

Supplementary Information

The online version contains supplementary material available at https://doi.org/10.1186/s12951-024-02897-4.

Supplementary Material 1

Supplementary Material 2

Acknowledgements
We would like to thank all donors and patients who participated in the study without whom this work would not have been possible. We thank Oili Suvi for excellent technical assistance. We would like to thank enGenome team for bioinformatics analysis and support.

Author contributions
CM: Design of the work, acquisition and interpretation of the data on HFnCUR, preparation of the original draft the work; VT: preparation of HFnCUR; PS: acquisition and analysis of data on the toxicological profile of HFnCUR; MT: design acquisition and analysis of data on the BBB; RD, DF, GP: acquisition and analysis of transcriptomics data on treated PBMCs; MF: acquisition and analysis of data on the 5xFAD mice; JA: acquisition and analysis of data on the 5xFAD mice; BN: acquisition and analysis of data on the 5xFAD mice; BL: acquisition and analysis of data on the 5xFAD mice; LB: preparation of HFnCUR; SN: design acquisition and analysis of data on the BBB; AT: design of the work, interpretation of the toxicological data; CC: design of the work and funding acquisition; SM: interpretation of the data on HFnCUR preparation and stability; DP: design of the work and funding acquisition; MAH: design of the work, interpretation of data from 5xFAD mice, preparation of the original draft the work, and funding acquisition; FC: design of the work and funding acquisition; SG: design of the work, interpretation of transcriptomics data on treated PBMCs, preparation of the original draft the work and funding acquisition. All authors read and approved the final manuscript.

Funding
This project supported by, the Estonian Research Council and from the General Secretariat for Research and Technology of Greece under the framework of EuroNanoMed III JTC 2018 project name: "CurcumAGE". This study was also funded by Ricerca Corrente 2022–2024, Italian Ministry of Health.

Data availability
The datasets in transcriptomics analysis used in this manuscript can be found at GEO repository (GSE203408).

Declarations

Ethics approval and consent to participate
All procedures performed in studies involving human participants were in accordance with the ethical standards of the institutional and/or national research committee and with the Helsinki declaration and its later amendments or comparable ethical standards. The study design was examined by the IRBs of the enrolling institutions. The study protocol to obtain blood from patients was approved by the Ethical Committee of the IRCCS Mondino Foundation (Pavia, Italy) (Code: 20170001758). Informed consent was obtained from all subjects involved in the study.

Consent for publication
Not applicable.

Competing interests
The authors declare no competing interests.

Author details
[1]Istituti Clinici Scientifici Maugeri IRCCS, Pavia 27100, Italy
[2]Department of Biotechnology and Bioscience, University of Milano-Bicocca, Piazza della Scienza 2, Milano 20126, Italy
[3]Department of Toxicology & Forensic Sciences, Faculty Medicine, University of Crete, Heraklion, Greece
[4]Department of Biology and Biotechnology "L. Spallanzani", University of Pavia, Pavia, Italy
[5]IRCCS Mondino Foundation, Pavia 27100, Italy
[6]Department of Pharmacology, Institute of Biomedicine and Translational Medicine, University of Tartu, Tartu, Estonia
[7]Department of Histology-Embryology, School of Medicine, University of Crete, Heraklion 71003, Greece
[8]Department of Biomedical and Clinical Sciences, Università di Milano, Milan 20157, Italy
[9]Center of Functional Genomics and Rare diseases, Department of Pediatrics, Buzzi Children's Hospital, Milan 20154, Italy

Received: 4 July 2024 / Accepted: 2 October 2024
Published online: 17 November 2024

References

1. Golde TE, Levey AI. Immunotherapies for Alzheimer's disease. Science. 2023;382:1242–4.
2. Rodrigue KM, Kennedy KM, Devous MD, Rieck JR, Hebrank AC, Diaz-Arrastia R, et al. β-Amyloid burden in healthy aging: Regional distribution and cognitive consequences. Neurology. 2012;78:387–95.
3. Hampel H, Hardy J, Blennow K, Chen C, Perry G, Kim SH, et al. The Amyloid-β pathway in Alzheimer's Disease. Mol Psychiatry. 2021;26:5481–503.
4. Mir RH, Shah AJ, Mohi-ud-din R, Pottoo FH, Dar MA, Jachak SM, et al. Natural anti-inflammatory compounds as drug candidates in Alzheimer's Disease. Curr Med Chem. 2021;28:4799–825.
5. Gagliardi S, Morasso C, Stivaktakis P, Pandini C, Tinelli V, Tsatsakis A, et al. Curcumin formulations and trials: what's New in Neurological diseases. Molecules. 2020;25:5389.
6. Gagliardi S, Truffi M, Tinelli V, Garofalo M, Pandini C, Cotta Ramusino M, et al. Bisdemethoxycurcumin (BDC)-Loaded H-Ferritin-nanocages mediate the regulation of inflammation in Alzheimer's Disease patients. Int J Mol Sci. 2022;23:9237.
7. Utomo RY, Sugie A, Okada S, Miura K, Nakamura H. Detoxification of amyloid β fibrils by curcumin derivatives and their verification in a *Drosophila* Alzheimer's model. Chem Commun. 2022;58:2576–9.
8. Gagliardi S, Franco V, Sorrentino S, Zucca S, Pandini C, Rota P, et al. Curcumin and Novel Synthetic analogs in cell-based studies of Alzheimer's Disease. Front Pharmacol. 2018;9:1404.
9. Seady M, Fróes FT, Gonçalves CA, Leite MC. Curcumin modulates astrocyte function under basal and inflammatory conditions. Brain Res. 2023;1818:148519.
10. Long JM, Holtzman DM. Alzheimer Disease: an update on pathobiology and treatment strategies. Cell. 2019;179:312–39.
11. Yang H-S, Teng L, Kang D, Menon V, Ge T, Finucane HK, et al. Cell-type-specific Alzheimer's disease polygenic risk scores are associated with distinct disease processes in Alzheimer's disease. Nat Commun. 2023;14:7659.
12. Schlepckow K, Morenas-Rodríguez E, Hong S, Haass C. Stimulation of TREM2 with agonistic antibodies—an emerging therapeutic option for Alzheimer's disease. Lancet Neurol. 2023;22:1048–60.

13. Peng Y, Ao M, Dong B, Jiang Y, Yu L, Chen Z, et al. Anti-inflammatory effects of Curcumin in the inflammatory diseases: Status, limitations and countermeasures. Drug Des Devel Ther. 2021;15:4503–25.
14. Kothawade SM, Buttar HS, Tuli HS, Kaur G. Therapeutic potential of flavonoids in the management of obesity-induced Alzheimer's disease: an overview of preclinical and clinical studies. Naunyn Schmiedebergs Arch Pharmacol. 2023;396:2813–30.
15. Tsuda T. Curcumin as a functional food-derived factor: degradation products, metabolites, bioactivity, and future perspectives. Food Funct. 2018;9:705–14.
16. Mainini F, Bonizzi A, Sevieri M, Sitia L, Truffi M, Corsi F, et al. Protein-based nanoparticles for the imaging and treatment of solid tumors: the case of Ferritin Nanocages, a Narrative Review. Pharmaceutics. 2021;13:2000.
17. Montemiglio LC, Testi C, Ceci P, Falvo E, Pitea M, Savino C, et al. Cryo-EM structure of the human ferritin–transferrin receptor 1 complex. Nat Commun. 2019;10:1121.
18. Fan K, Jia X, Zhou M, Wang K, Conde J, He J, et al. Ferritin Nanocarrier traverses the blood brain barrier and kills glioma. ACS Nano. 2018;12:4105–15.
19. Fiandra L, Mazzucchelli S, Truffi M, Bellini M, Sorrentino L, Corsi F. In Vitro Permeation of FITC-loaded ferritins across a rat blood-brain barrier: a model to study the delivery of Nanoformulated Molecules. J Vis Exp. 2016;54279.
20. Pandolfi L, Bellini M, Vanna R, Morasso C, Zago A, Carcano S, et al. H-Ferritin enriches the Curcumin Uptake and improves the therapeutic efficacy in Triple negative breast Cancer cells. Biomacromolecules. 2017;18:3318–30.
21. Oakley H, Cole SL, Logan S, Maus E, Shao P, Craft J, et al. Intraneuronal β-Amyloid aggregates, neurodegeneration, and Neuron Loss in Transgenic Mice with five familial Alzheimer's disease mutations: potential factors in amyloid plaque formation. J Neurosci. 2006;26:10129–40.
22. Oblak AL, Lin PB, Kotredes KP, Pandey RS, Garceau D, Williams HM, et al. Comprehensive evaluation of the 5XFAD mouse model for preclinical testing applications: a MODEL-AD study. Front Aging Neurosci. 2021;13:713726.
23. O'Leary TP, Brown RE. Visuo-spatial learning and memory impairments in the 5xFAD mouse model of Alzheimer's disease: effects of age, sex, albinism, and motor impairments. Genes Brain Behav. 2022;21:e12794.
24. Faisal M, Aid J, Nodirov B, Lee B, Hickey MA. Preclinical trials in Alzheimer's disease: Sample size and effect size for behavioural and neuropathological outcomes in 5xFAD mice. Burne TH, editor. PLOS ONE. 2023;18:e0281003.
25. Percie Du Sert N, Ahluwalia A, Alam S, Avey MT, Baker M, Browne WJ, et al. Reporting animal research: explanation and elaboration for the ARRIVE guidelines 2.0. Boutron I, editor. PLOS Biol. 2020;18:e3000411.
26. Truffi M, Fiandra L, Sorrentino L, Monieri M, Corsi F, Mazzucchelli S. Ferritin nanocages: a biological platform for drug delivery, imaging and theranostics in cancer. Pharmacol Res. 2016;107:57–65.
27. Li B, Dewey CN. RSEM: accurate transcript quantification from RNA-Seq data with or without a reference genome. BMC Bioinformatics. 2011;12:323.
28. Leng N, Dawson JA, Thomson JA, Ruotti V, Rissman AI, Smits BMG, et al. EBSeq: an empirical Bayes hierarchical model for inference in RNA-seq experiments. Bioinformatics. 2013;29:1035–43.
29. Anders S, McCarthy DJ, Chen Y, Okoniewski M, Smyth GK, Huber W, et al. Count-based differential expression analysis of RNA sequencing data using R and Bioconductor. Nat Protoc. 2013;8:1765–86.
30. Love MI, Huber W, Anders S. Moderated estimation of Fold change and dispersion for RNA-seq data with DESeq2. Genome Biol. 2014;15:550.
31. Kyoto Encyclopedia of Genes and Genomes [Internet]. http://www.genome.ad.jp/kegg
32. Kuleshov MV, Jones MR, Rouillard AD, Fernandez NF, Duan Q, Wang Z, et al. Enrichr: a comprehensive gene set enrichment analysis web server 2016 update. Nucleic Acids Res. 2016;44:W90–7.
33. Vorhees CV, Williams MT. Morris water maze: procedures for assessing spatial and related forms of learning and memory. Nat Protoc. 2006;1:848–58.
34. Theparambil SM, Hosford PS, Ruminot I, Kopach O, Reynolds JR, Sandoval PY, et al. Astrocytes regulate brain extracellular pH via a neuronal activity-dependent bicarbonate shuttle. Nat Commun. 2020;11:5073.
35. Rizzuto MA, Dal Magro R, Barbieri L, Pandolfi L, Sguazzini-Viscontini A, Truffi M, et al. H-Ferritin nanoparticle-mediated delivery of antibodies across a BBB *in vitro* model for treatment of brain malignancies. Biomater Sci. 2021;9:2032–42.
36. Sevieri M, Mazzucchelli S, Barbieri L, Garbujo S, Carelli S, Bonizzi A, et al. Ferritin nanoconjugates guide trastuzumab brain delivery to promote an antitumor response in murine HER2 + breast cancer brain metastasis. Pharmacol Res. 2023;196:106934.
37. Yoo C-H, Kim J, Baek H-M, Chang K-A, Choe B-Y. Neurodegenerative changes in the brains of the 5xFAD Alzheimer's Disease Model mice investigated by high-field and high-resolution magnetic resonance imaging and Multi-nuclei magnetic resonance spectroscopy. Int J Mol Sci. 2023;24:5073.
38. Seo N-Y, Kim GH, Noh JE, Shin JW, Lee CH, Lee KJ. Selective Regional loss of cortical synapses lacking presynaptic mitochondria in the 5xFAD Mouse Model. Front Neuroanat. 2021;15:690168.
39. Lu Y, Fujioka H, Wang W, Zhu X. Bezafibrate confers neuroprotection in the 5xFAD mouse model of Alzheimer's disease. Biochim Biophys Acta Mol Basis Dis. 2023;1869:166841.
40. Rejc L, Gómez-Vallejo V, Joya A, Arsequell G, Egimendia A, Castellnou P, et al. Longitudinal evaluation of neuroinflammation and oxidative stress in a mouse model of Alzheimer disease using positron emission tomography. Alzheimers Res Ther. 2022;14:80.
41. Xu Y, Gao W, Sun Y, Wu M. New insight on microglia activation in neurodegenerative diseases and therapeutics. Front Neurosci. 2023;17:1308345.
42. Keren-Shaul H, Spinrad A, Weiner A, Matcovitch-Natan O, Dvir-Szternfeld R, Ulland TK, et al. A Unique Microglia Type Associated with Restricting Development of Alzheimer's Disease. Cell. 2017;169:1276–e129017.
43. Reddy PH, Manczak M, Yin X, Grady MC, Mitchell A, Kandimalla R, et al. Protective effects of a natural product, Curcumin, against amyloid β Induced mitochondrial and synaptic toxicities in Alzheimer's Disease. J Investig Med. 2016;64:1220–34.
44. Mazzanti G, Di Giacomo S. Curcumin and Resveratrol in the management of Cognitive disorders: what is the clinical evidence? Molecules. 2016;21:1243.
45. Kuszewski JC, Wong RHX, Howe PRC. Can Curcumin counteract Cognitive decline? Clinical trial evidence and rationale for combining ω-3 fatty acids with Curcumin. Adv Nutr. 2018;9:105–13.
46. Nelson KM, Dahlin JL, Bisson J, Graham J, Pauli GF, Walters MA. The essential Medicinal Chemistry of Curcumin: Miniperspective. J Med Chem. 2017;60:1620–37.
47. Nelson KM, Dahlin JL, Bisson J, Graham J, Pauli GF, Walters MA. Curcumin May (not) defy Science. ACS Med Chem Lett. 2017;8:467–70.
48. Quick JD, Silva C, Wong JH, Lim KL, Reynolds R, Barron AM, et al. Lysosomal acidification dysfunction in microglia: an emerging pathogenic mechanism of neuroinflammation and neurodegeneration. J Neuroinflammation. 2023;20:185.
49. Luss AL, Bagrov DV, Yagolovich AV, Kukovyakina EV, Khan II, Pokrovsky VS, et al. Toxicity evaluation and controlled-release of curcumin-loaded amphiphilic Poly-N-vinylpyrrolidone nanoparticles: in Vitro and in vivo models. Pharmaceutics. 2023;16:8.
50. Shajari M, Zamani M, Ahmadi N, Rostamizadeh K, Shapouri R. Improving the antibacterial activity of Curcumin Loaded nanoparticles in Wastewater Treatment by enhancing permeability and sustained release. J Polym Environ. 2022;30:2658–68.
51. Karzi V, Ozcagli E, Tzatzarakis MN, Vakonaki E, Fragkiadoulaki I, Kalliantasi A, et al. DNA damage estimation after chronic and combined exposure to endocrine disruptors: an in vivo real-life risk Simulation Approach. Int J Mol Sci. 2023;24:9989.
52. Tsatsakis A, Docea AO, Constantin C, Calina D, Zlatian O, Nikolouzakis TK, et al. Genotoxic, cytotoxic, and cytopathological effects in rats exposed for 18 months to a mixture of 13 chemicals in doses below NOAEL levels. Toxicol Lett. 2019;316:154–70.
53. Wu D, Chen Q, Chen X, Han F, Chen Z, Wang Y. The blood–brain barrier: structure, regulation, and drug delivery. Signal Transduct Target Ther. 2023;8:217.
54. Banks WA. Drug delivery to the brain in Alzheimer's disease: consideration of the blood–brain barrier. Adv Drug Deliv Rev. 2012;64:629–39.
55. La Rosa F, Zoia CP, Bazzini C, Bolognini A, Saresella M, Conti E, et al. Modulation of MAPK- and PI3/AKT-Dependent Autophagy Signaling by Stavudine (D4T) in PBMC of Alzheimer's Disease patients. Cells. 2022;11:2180.
56. Kurt S, Tomatir AG, Tokgun PE, Oncel C. Altered expression of long non-coding RNAs in Peripheral Blood mononuclear cells of patients with Alzheimer's Disease. Mol Neurobiol. 2020;57:5352–61.
57. Chakraborty A, Sami SA, Marma KKS. A comprehensive review on RAGE-facilitated pathological pathways connecting Alzheimer's disease, diabetes mellitus, and cardiovascular diseases. Egypt J Intern Med. 2021;33:47.
58. Rudajev V, Novotny J. Cholesterol as a key player in amyloid β-mediated toxicity in Alzheimer's disease. Front Mol Neurosci. 2022;15:937056.
59. Pantelopulos GA, Abraham CB, Straub JE. Cholesterol and lipid rafts in the Biogenesis of Amyloid-β protein and Alzheimer's Disease. Annu Rev Biophys. 2024;53:annurev–biophys.
60. Eimer WA, Vassar R. Neuron loss in the 5XFAD mouse model of Alzheimer's disease correlates with intraneuronal Aβ42 accumulation and Caspase-3 activation. Mol Neurodegener. 2013;8:2.

61. Zhang G, Wang Z, Hu H, Zhao M, Sun L. Microglia in Alzheimer's Disease: a target for therapeutic intervention. Front Cell Neurosci. 2021;15:749587.
62. Carter SF, Herholz K, Rosa-Neto P, Pellerin L, Nordberg A, Zimmer ER. Astrocyte biomarkers in Alzheimer's Disease. Trends Mol Med. 2019;25:77–95.
63. Mancuso R, Fryatt G, Cleal M, Obst J, Pipi E, Monzón-Sandoval J, et al. CSF1R inhibitor JNJ-40346527 attenuates microglial proliferation and neurodegeneration in P301S mice. Brain. 2019;142:3243–64.
64. Begum AN, Jones MR, Lim GP, Morihara T, Kim P, Heath DD, et al. Curcumin Structure-Function, bioavailability, and efficacy in models of Neuroinflammation and Alzheimer's Disease. J Pharmacol Exp Ther. 2008;326:196–208.
65. Sundaram JR, Poore CP, Sulaimee NHB, Pareek T, Cheong WF, Wenk MR, et al. Curcumin ameliorates Neuroinflammation, Neurodegeneration, and memory deficits in p25 Transgenic Mouse Model that bears hallmarks of Alzheimer's Disease. J Alzheimers Dis. 2017;60:1429–42.

Publisher's note